Carbon Spheres Assisted Synthesis of Porous Bioactive Glass Containing Hydroxycarbonate Apatite Nanocrystals: a Material with High in Vitro Bioactivity

Dinesh Jagadeesan,[†] C. Deepak,[‡] Kavitha Siva,[§] Maneesha S. Inamdar,[§] and M. Eswaramoorthy*[,†]

Chemistry and Physics of Materials Unit, DST Unit on Nanoscience, Jawaharlal Nehru Centre for Advanced Scientific Research, Jakkur, Bangalore, 560064. India. National Institute of Technology, Surathkal, 575025. India. and Molecular Biology and Genetics Unit, Jawaharlal Nehru Centre for Advanced Scientific Research, Jakkur, Bangalore, 560064. India

Received: December 17, 2007; In Final Form: March 3, 2008

A hierarchically porous bioactive glass of composition 80 mol % SiO_2 and 15 mol % CaO (MBGH) was synthesized using pluoronic P123 and glucose-derived amorphous carbon spheres as templates. While the carbon spheres leave behind pores of 300 nm to a few micrometers after calcination, the walls of these pores contain orderly arranged mesopores of 3−5 nm orchestrated by the pluoronic polymer. The role of carbon spheres is not only to create pores but also to aid in increased growth rate of hydroxycarbonate apatite in simulated body fluid (SBF). The negatively charged carbon spheres favor the local enrichment of calcium ions and facilitate the formation of amorphous calcium phosphate around the surface. On calcination, the walls of the macropores contain crystalline hydroxycarbonate apatite nuclei. MBGH also exhibits an accelerated growth of monoclinic-like apatite in SBF. The in vitro activity has been studied by XRD, FT-IR, FESEM, and TEM.

Introduction

Bioactive glass ceramics of composition $CaO-P_2O_5-SiO_2-MO$ (M = Na, Mg, etc.) are much sought after materials in tissue engineering due to their ability to form chemical bonds with the bone through the formation of biologically compatible hydroxycarbonate apatite (HCA), when implanted in the body.[1] Findings that the bioactive glasses can also upregulate different genes of primary human osteoblast cells evoke a great deal of interest in such materials.[2] The efficiency of a bioactive glass greatly depends on the rate at which HCA forms on its surface in the presence of the body fluid. When the rate of formation of HCA is slow, no bond forms, and the material is no longer bioactive. Hence, there have been continuous efforts to develop materials with enhanced rate of HCA growth in the body fluid in order to blend well with the bone. A layer of HCA can also form on the bioglass when soaked in a simulated body fluid (SBF). Thus, the formation rate of HCA in SBF, sometimes referred to as in vitro bioactivity, can be used to predict the performance of the material when implanted in the body. The classical melt-derived bioglass takes a month-long time in SBF to crystallize apatite on their surface.[3,4] On the other hand, sol−gel derived bioglasses are able to crystallize HCA within 5−15 days time owing to their reactive silanol groups and increased porosity.[5,6] The presence of a highly soluble $NaCaPO_4$ phase coexisting with hydroxyapatite was recently reported to have very high in vitro bioactivity.[7] A recent report claims that mesostructured bioglass (MBG) is a better candidate for the fast crystallization of HCA in 8 h in SBF.[8] Here we report the synthesis of hierarchically porous MBGH showing exceptional growth for monoclinic-like HCA in SBF in a very short period of less than 1 h. The hierarchy in the porosity arises from the macropores (300−800 nm) with their walls made of orderly arranged mesopores (3−5 nm). The former is templated by glucose-derived carbon spheres, and the latter is templated by the pluoronic polymer. Though attempts were made in the past to obtain hierarchically porous bioactive glass,[9,10] the MBGH described here is an inherently premixed nanocomposite of HCA nanocrystals (again induced by carbon spheres) in a mesoporous silica matrix. This is very different from the existing glass-reinforced apatites[11] where the composites are usually obtained by physical mixing of the bioactive glass powder and synthetic hydroxyapatite crystals at microscale. Having a nanocomposite can offer many advantages besides the fact that such a material would closely resemble the natural bone. HCA nanocrystals in the matrix serve as nuclei for the further growth of HCA in SBF. The macropores described in MBGH can also be expected to enhance the cell adhesion due to increased roughness on the surface[12] and also aid in an efficient diffusion of macromolecules in physiological environment. Hence, these materials could be ideal as coatings along the walls of the existing macroporous (>100 μm) biopolymer scaffolds to have an improved in vivo performance as bone implants. Further, their ability to form monoclinic-like HCA under in vitro conditions places hope on the bioelectric effects on bone growth.[13]

Experimental Section

Synthesis of Amorphous Carbon Additive. 2.02 g of glucose was dissolved in 8 mL of water, and an equal volume of *n*-octane was added to it. The whole mixture was kept at 180 °C in a sealed 25-mL Teflon-lined stainless steel autoclave.

* To whom correspondence should be addressed. Fax: 91-080-22082766. Tel: 91-080-22082870. E-mail: eswar@jncasr.ac.in.
[†] Chemistry and Physics of Materials Unit, DST Unit on Nanoscience, Jawaharlal Nehru Centre for Advanced Scientific Research.
[‡] National Institute of Technology.
[§] Molecular Biology and Genetics Unit, Jawaharlal Nehru Centre for Advanced Scientific Research.

10.1021/jp800850m CCC: $40.75
Published on Web 04/16/2008

After 14 h, the autoclave was cooled naturally to room temperature. The octane layer was decanted, and the dark brown paste found at the bottom of the container was carefully collected and stirred in ethanol for 2 h. The carbon spheres (brown solid) were separated by centrifugation at 5000 rpm for 10 min and dried at 80 °C in air for 4 h. The size of the as-synthesized carbon spheres was in the range of 300 nm to a few micrometer (Supporting Information, Figure S1).

Synthesis of Hierarchically Porous Bioactive Glass. A general protocol for the synthesis of MBGH involved making a slurry of carbon spheres with calcium and phosphorus containing silica sol. The silica sol was prepared by the following procedure.[8] P123 (4.0 g), tetraethyl orthosilicate, 6.7 g, $Ca(NO_3)_2 \cdot 4H_2O$ (1.4 g), triethyl phosphate (0.73 g), and 0.5 M HCl (1.0 g) were dissolved in ethanol (60 g) and stirred in a closed beaker at room temperature for 1 day. The slurry was obtained by physically mixing the carbon spheres and silica sol in a definite ratio. The slurry was allowed to dry at room temperature for 6 h to aid the evaporation-induced self-assembly process of block copolymer (P123) to form a mesostructure around the carbon spheres. The dried powder was calcined at 700 °C for 5 h to obtain the final MBGH products. MBG was prepared in a similar way except that the carbon spheres were not added to the initial silica sol.

In Vitro Studies. In vitro studies were performed by soaking the powder samples of MBGH in a modified SBF (40 mg in 40 mL) prepared according to the procedure reported in the literatutre.[14] Samples were soaked in SBF at 37 °C and pH 7.22 over a period of 1 h, 3 h, 6 h, 12 h, 3 days, and 14 days. Accordingly, the samples were labeled as MBGH-1h, MBGH-3h, MBGH-6h, MBGH-12h, MBGH-3d, and MBGH-2w. Finally, the samples were recovered by filtration using a 200-nm-pore polycarbonate membrane (Millipore GTTP04700), washed three times with acetone, and dried in air for 1 h.

Sample Characterization. The morphology of the samples was analyzed by a field emission scanning electron microscope (FESEM, FEI Nova-Nano SEM-600). TEM images were recorded with a JEOL JEM 3010 instrument operated with an accelerating voltage of 300 kV. Low-angle X-ray diffraction characterization was done at 25 °C with a Rich-Siefert 3000-TT diffractometer employing Cu Kα radiation. Wide-angle X-ray diffraction (XRD) characterization was done at 25 °C with a Bruker-D8 X-ray diffractometer employing Cu Kα radiation. FT-IR was recorded on a KBr pellet (sample to KBr ratio, 1:80). N_2 adsorption−desorption isotherms were measured at 77 K using a Quantachrome Autosorb-1C instrument.

Results and Discussion

Figure 1a shows the wide-angle XRD pattern of the MBG and MBGH samples after calcination. Unlike MBG, MBGH shows reflections for hydroxyapatite nanocrystals at 2θ; 25.8°, 31.7°, and 32.9°. However, it would be difficult to assign these peaks to a particular phase (hexagonal or monoclinic) of hydroxyapatite as there are only a limited number of reflections in the XRD pattern. The low-angle peak observed at $2\theta = 1.19°$ for MBG and at 1.04° for MBGH (Figure 1b) is associated with ordered arrangement of the mesopores in the silica matrix. It suggests that the presence of carbon spheres did not affect self-assembly of pluronic polymer P123 to form ordered mesopores. Figure 1c shows the FESEM image of MBGH exhibiting macropores of size 200 nm to a few micrometers templated by the carbon spheres (see also Supporting Information, Figure S2). The density of the macropores could be increased by increasing the amount of carbon spheres used to form the slurry. A magnified image of the sponge-like structure of MBGH is shown in the inset of Figure 1c. TEM image of the fragmented wall shows uniform mesoporous channels viewed perpendicular to the channel direction (Supporting Information, Figure S3). The TEM image in Figure 1d further reveals the presence of dark contrast crystals of 5−20 nm in size (indicated by white arrows) specifically located in and around the macropores of MBGH templated by the carbon spheres. The selected area electron diffraction pattern (Figure 1e) displays a polycrystalline pattern, typical of hydroxyapatite nanocrystals. The HREM image (Figure 1f) of a crystal shows the lattice spacing of 0.280 nm charcteristic of a hydroxyapatite crystal.

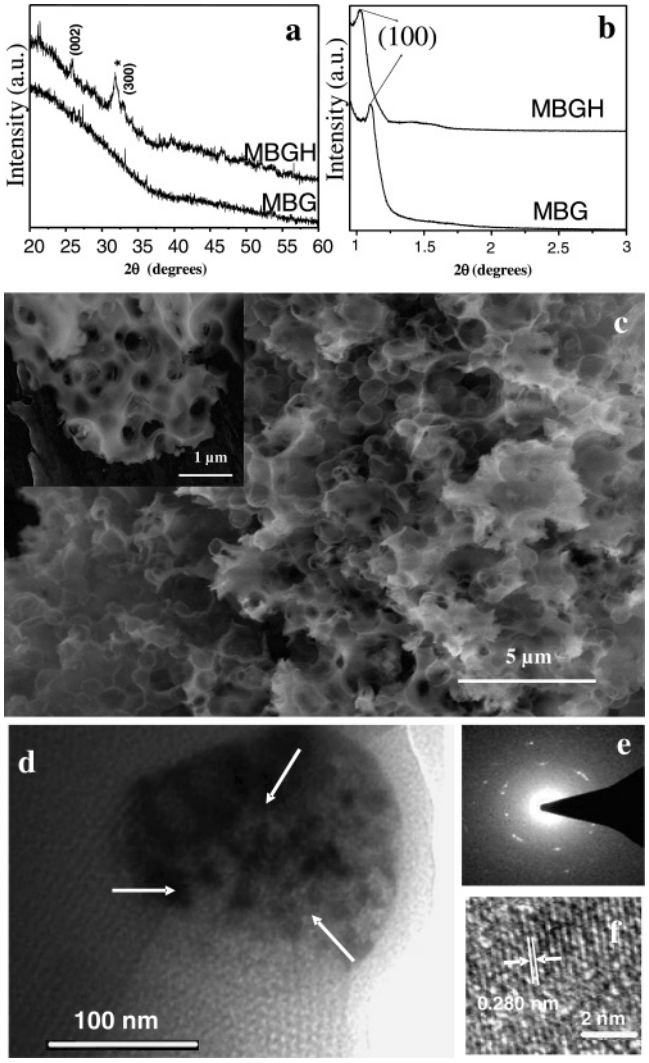

Figure 1. (a) Wide-angle XRD pattern of calcined MBG and MBGH samples. * This peak can be assigned to either the (211) plane of hexagonal or (221) plane of monoclinic phase of HCA. (b) Low-angle XRD pattern of MBG and MBGH. (c) FESEM image of MBGH showing macropores. Inset shows the magnified image of MBGH. (d) TEM image of MBGH showing HCA nanocrystals (patches of dark contrast indicated by arrow marks) around the macropore region (e) corresponding ED pattern. (f) HREM image of an HCA nanocrystal.

Nitrogen sorption isotherms of calcined MBG and MBGH samples showed a type IV isotherm with H1-type hysterisis identified with the cylindrical mesopores (Supporting Information, Figure S4). The pore volume (at $P/P_0 = 0.98$) and pore size of MBGH obtained from nitrogen adsorption isotherm were 0.49 cm^3/g and 5 nm, respectively. The low BET surface area

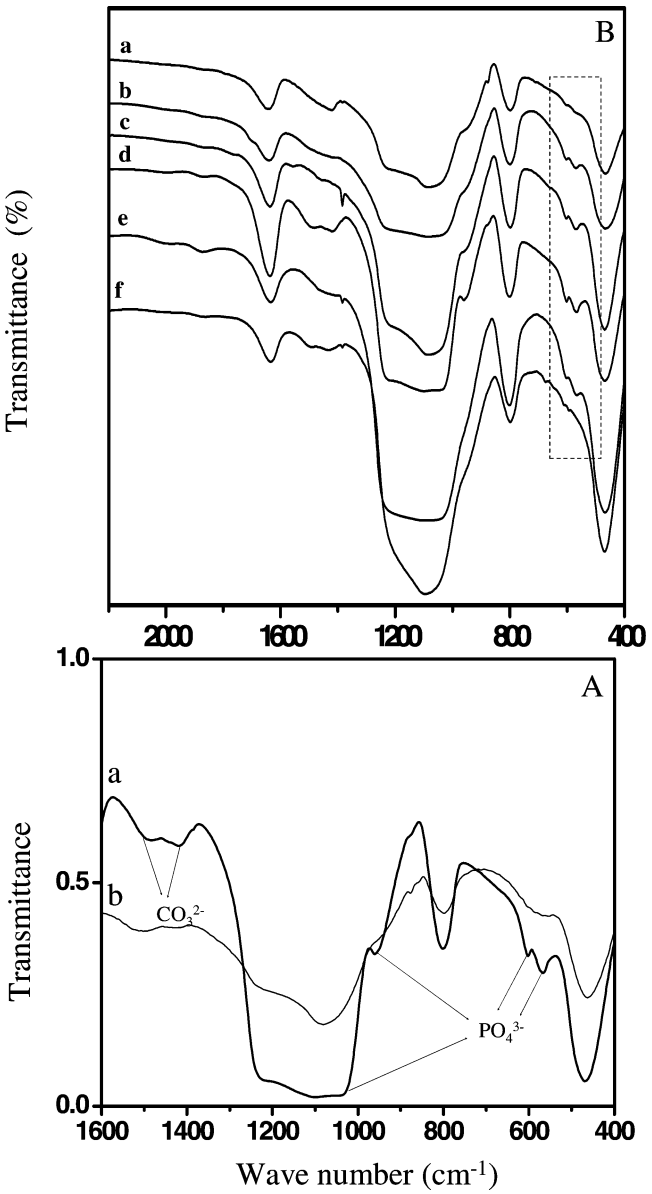

Figure 2. (A) FT-IR of (a) calcined MBGH and (b) calcined MBG before soaking in SBF. (B) FT-IR studies of MBGH prepared with various carbon sphere content. (a) Blank (no carbon spheres) and C/Ca weight ratio (b) 0.5, (c) 4, (d) 10, (e) 50, and (f) 500.

($270\ m^2/g$) obtained for MBGH compared to the MBG sample ($351\ m^2/g$) is attributed to the presence of macropores.

FT-IR spectra of MBG and MBGH are compared in Figure 2A. The O−P−O bending frequencies at 600−570 cm^{-1} and P−O stretching frequency at 960 cm^{-1} are present only in the case of MBGH. The bands at 1490 and 1423 cm^{-1} seen in MBGH correspond to CO_3^{2-} stretching frequencies. Thus, FT-IR also confrms the presence of crystals of HCA in MBGH. Synthesis of MBGH at different weight ratios of carbon spheres to calcium nitrate (C/Ca = 0, 0.5, 4, 10, 50, and 500) was carried out and their FT-IR spectrum after calcination is presented in the Figure 2B. The O−P−O bending frequency region from 600 to 570 cm^{-1} was monitored to study the formation of crystalline HCA at different carbon content. The initial increase in intensity of HCA bands at 568 and 603 cm^{-1} with increase in the C/Ca ratio (from 0.5 to 10) confirms the role of carbon spheres in the formation of crystalline HCA nuclei. At higher ratios (C/Ca = 50 and above) the distinction between the two bands disappeared.

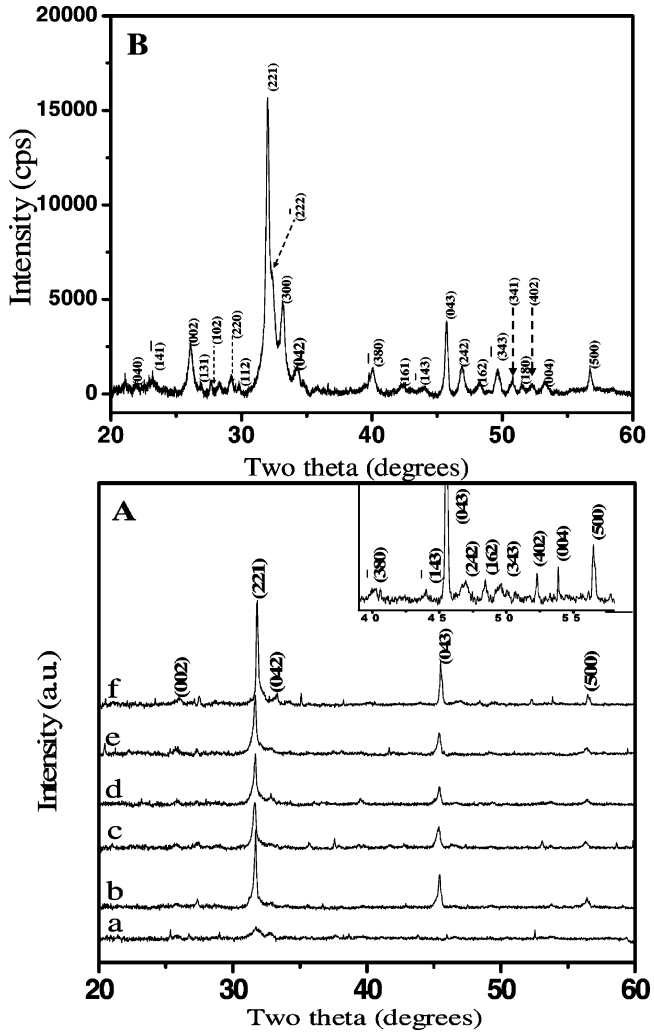

Figure 3. (A) XRD patterns of (a) calcined MBGH (without SBF treatment), and MBGH soaked in SBF for various periods of time: (b) 1 h, (c) 3 h, (d) 6 h, (e) 12 h, and (f) 3 days. Inset shows the magnified (twice) pattern of (f) in the 2θ range from 38° to 60°. (B) XRD of MBGH soaked in SBF for 2 weeks, indexed to monoclinic HCA.

The growth of HCA crystals on the surface of MBGH (C/Ca ratio = 10) soaked in SBF at different periods of time was monitored using XRD, and the results are shown in Figure 3A. The integral intensity of the peak at 2θ 31.7° corresponding to (221) was found to increase 4.5 times within 10 min of soaking in SBF (Supporting Information, Figure S5). In a 1-h period, two prominent peaks at 2θ range 31.7° and 45.3° followed by a very weak peak at 56.3° emerged. Increasing the soaking time from 1 to 12 h did not show any significant change in the intensity of XRD peaks, indicating a slowdown in the rate of crystal growth. Samples soaked for a longer period of time (3 days) showed an increase in intensity for the original peaks along with some additional peaks (Figure 3A inset) that could be indexed to monoclinic HCA. The calculated pattern for the samples soaked in SBF for less than 24 h also fits well for the monoclinic rather than the hexagonal phase. MBGH soaked in SBF for 2 weeks showed very well resolved peaks indexed to monoclinic HCA (Figure 3B). The peaks were indexed using the program DICVOL91 TREOR90 in CRYSFIRE. No best solutions were obtained when the indexing was restricted to the hexagonal phase (P63/m) but yielded solutions to monoclinic

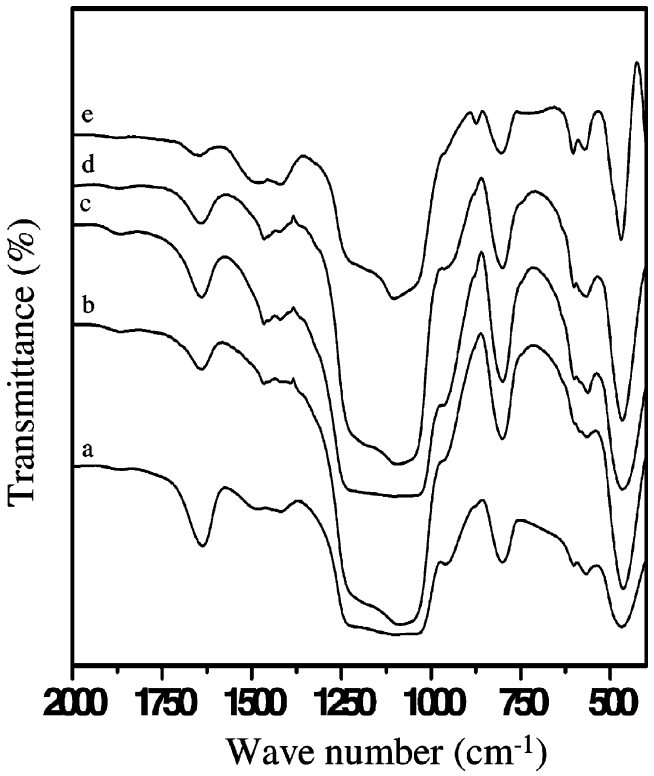

Figure 4. FT-IR spectrum of (a) calcined MBGH, and MBGH soaked in SBF at different periods of time: (b) 1 h, (c) 12 h, (d) 3 days, and (e) 2 weeks.

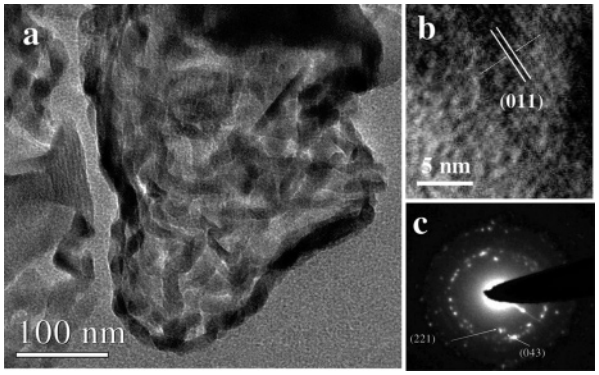

Figure 5. (a) TEM image of hollow structure of MBGH-1h showing the HCA crystals. (b) HREM of the crystal. (c) SAED pattern of the HCA crystal.

phase (JCPDF 76-0694). The XRD patterns were further refined for the cell parameters using TOPAS (Supporting Information, Figure S6).

In Figure 4, we show the FT-IR spectra of MBGH before and after soaking in SBF at different periods of time. The O−P−O bending frequency region showed two distinguishable bands for the samples soaked in SBF for 1 h. However, with increased time of soaking, the spectral region from 570 to 610 cm^{-1}displayed three broad bands. The restoring of three bands into two was observed in the sample soaked in SBF for over 2 weeks.

In Figure 5a, the TEM image of MBGH-1 h shows the presence of HCA crystals around 50−100 nm. The crystallinity of the samples was evident from the HREM image showing the (011) plane of HCA (Figure 5b). The electron diffraction pattern (Figure 5c) shows polycrystalline nature whose rings are indexed to (221) and (043) planes of HCA. The macropores

SCHEME 1: Scheme Showing the Role of Carbon in the Formation of Hierarchically Porous Bioactive Glass

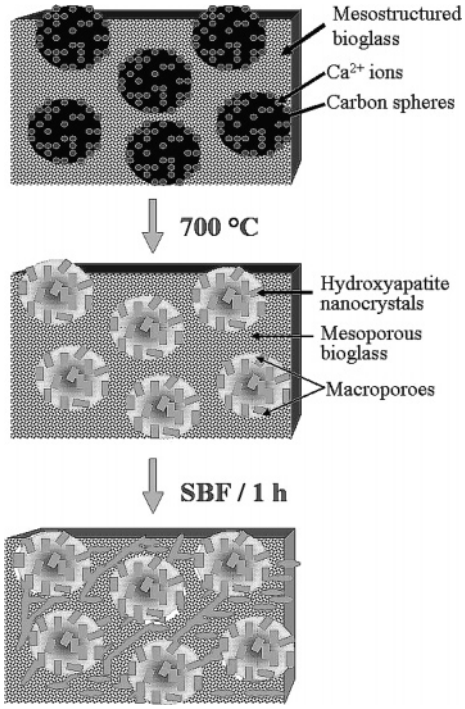

of MBGH are gradually covered with the nanocrystals of HCA on soaking for a longer duration in SBF as analyzed using FESEM as shown in Supporting Information, Figure S7.

The role of amorphous carbon sphere additive in obtaining HCA nuclei can be explained as follows. The carbon spheres possess a negatively charged surface with a ζ potential of −24 mV in water at pH 7.3. Besides, the FT-IR spectrum of the carbon spheres showed intense bands at 1702 and 3369 cm^{-1} corresponding to the presence of C═O and O−H stretches, respectively. Therefore, adsorption of divalent and trivalent metal ions on the surface of the carbon sphere is expected and has already been exploited to make metal oxide and nitride hollow structures.[15,16] In the present case, the negatively charged surface of the carbon spheres increases the local concentration of Ca^{2+} around them and facilitates the nucleation of calcium phosphates. The binding capacity of the carbon spheres with divalent calcium ions was studied by soaking the carbon spheres in calcium nitrate solution for 1 h followed by an extensive washing with water. Elemental mapping performed on these spheres showed the presence of calcium all over the surface (Supporting Information, Figure S8). The oxygen distribution comes from the functional groups located on the surface. Attempts to synthesize mesostructured silica in the absence of calcium nitrate were not successful due to the interference of charged surface of the carbon spheres on the formation of micelles. On the other hand, the presence of calcium ions passivates the surface charge of carbon spheres and hence allows the formation of micelles, a prerequisite to the development of mesostructure. Thus, the strong binding affinity of carbon spheres with calcium ions is unambiguously proved by elemental mapping. The conclusion also supports the results of FT-IR studies of MBGH synthesized at different carbon content. Besides, at higher ratios (C/Ca = 50 and above in Figure 2B), the distinction between the two bands disappeared, suggesting a substantial reduction in the localized concentration of calcium ions on each sphere, which, in turn, decreases the calcium phosphate formation in presence of phosphate ions. The

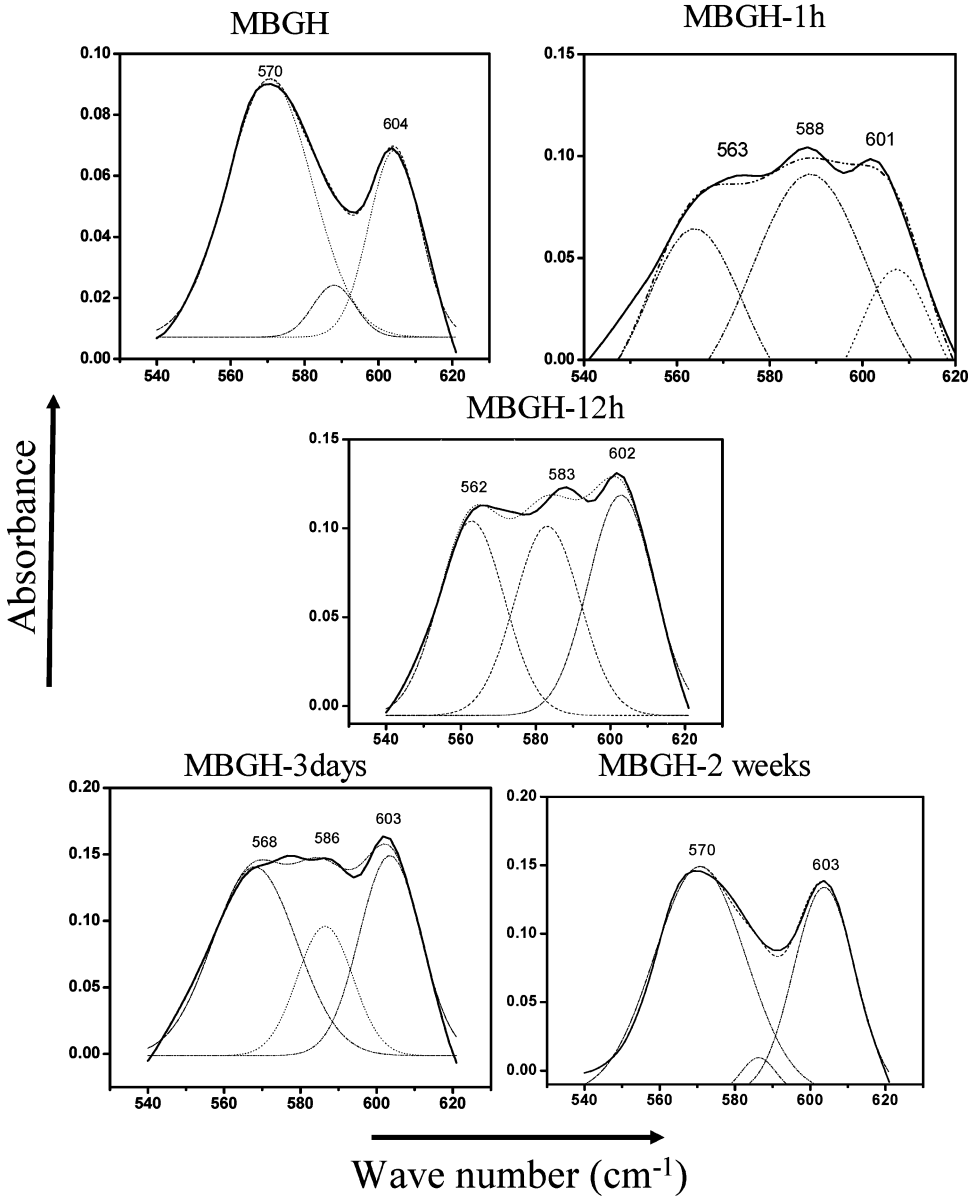

Figure 6. Deconvolution of FT-IR spectra of MBGH, MBGH-1h, MBGH-12h, MBGH-3d, and MBGH-2w.

enormous amount of heat generated locally during the exothermic reaction of calcination of carbon spheres plays a very important role in converting amorphous calcium phosphates into crystalline HCA in localized regions within macropores. XRD patterns of the carbon spheres soaked in bioactive silica sol for 6 h did not show any peak assigned to the crystalline HCA, indicating the importance of calcination (see Scheme 1).

The in vitro studies performed in SBF suggests a better performance of MBGH as compared to MBG and MBG treated with phosphate buffers.[17] XRD patterns of MBGH showed a considerable increase in the intensity of HCA crystals within 10 min of soaking in SBF. The very rapid growth of HCA in MBGH can be attributed to the presence of hydroxyapatite nuclei in the initial stage itself. However, with prolonged hours of soaking, the intensity of XRD peaks increased only slightly. The analysis of the FT-IR spectrum of the corresponding samples was informative. Amorphous calcium phosphates are known to give a broad band[18] in the region 600−570 cm^{-1}, while the crystalline phosphates exhibit two distinct bands at 570 and 604 cm^{-1} for O−P−O bending mode vibrations. The presence of two distinguishable bands at 570 and 604 cm^{-1} for the calcined MBGH sample clearly indicates the formation of HCA crystals nucleated by the carbon spheres. Soaking the sample in SBF for 1 h resulted in broadening of these bands possibly due to the formation of amorphous calcium phosphate in addition to crystalline HCA. The deconvoluted, O−P−O bending region shows three possible absorption bands with the broad, middle one being assigned to amorphous calcium phosphate (Figure 6). The decrease in intensity of the amorphous band with increase in soaking time is attributed to the transformation of amorphous calcium phosphate to crystalline form. This is further supported by the clear restoring of the O−P−O bending modes for MBGH soaked in the SBF for over 2 weeks. These data are in good agreement with XRD where a slowdown in the growth of crystalline HCA was observed with increased period of soaking in SBF. The eventual conversion of amorphous calcium phosphate into crystalline HCA is also substantiated from XRD recorded for the sample soaked in SBF for over 2 weeks.

Conclusion

We have synthesized hierarchically porous bioactive glass with improved bioactivity by employing glucose-derived amor-

phous carbon spheres as a template. The carbon spheres have been found to be instrumental in creating HCA nuclei. The high surface area derived from the mesopores and HCA nuclei derived from the carbon spheres are responsible for the enhanced in vitro bioativity. The preliminary biocompatibility test using human fibroblasts cells shows that the MBGH is not toxic to the cells (Supporting Information, Figure S9). Further experiments on the adhesion and differentiation of osteoblast cells on the surface of MBGH is under progress.

Acknowledgment. The authors thank Prof. C.N.R. Rao, FRS for his kind support and encouragement. They also thank Dr. A. Sundaresan (JNCASR) for useful discussion in analysing XRD results.

Supporting Information Available: TEM image of carbon spheres, FESEM image of MBG and MBGH, TEM image of MBGH, XRD of MBGH soaked in SBF for 10 min, surface area, profile matching of XRD of MBGH, 2 weeks, FESEM image of MBGH. 1 h, 3 d, 6 d, and 2 weeks, EDX mapping and biocompatibility tests. This material is available free of charge via the Internet at http://pubs.acs.org

References and Notes

(1) Hench, L. L. *J. Am. Ceram. Soc.* **1998**, *81*, 1705.

(2) Xynos, I. D.; Edgar, A. J.; Buttery, L. D. K.; Hench, L. L.; Polak, J. M. *J. Biomed. Mater.* Res. **2001**, *55*, 151.

(3) Hench, L. L.; Splinter, R. J.; Allen, W. C.; Greenlee, T. K., Jr. *J. Biomed. Mater. Res.* **1971**, *2*, 117.

(4) Ohura, K.; Nakamura, T.; Yamamuro, T.; Kokubo, T.; Ebisawa, Y.; Kotoura, Y.; Oka, M. *J. Biomed. Mater. Res.* **1991**, *25*, 357.

(5) Li, P.; Nakanishi, K.; Kokubo, T.; de Groot, K. *Biomaterials* **1993**, *14*, 963.

(6) Vallet-Regí, M.; Rámila, A. *Chem. Mater*. **2000**, *12*, 961.

(7) Andersson, J.; Johannessen, E.; Areva, S.; Baccile, N.; Azaïs, T.; Lindén, M. *J. Mater. Chem*, **2007**, *17*, 463.

(8) Yan, X.; Yu, C.; Zhou, X.; Tang, J.; Zhao, D. *Angew. Chem., Int. Ed.* **2004**, *43*, 5980.

(9) Yun, H. S.; Kim, S.; Hyeon, Y. *Chem. Commun*. **2007**, 2139.

(10) Li, X.; Wang, X.; Chen, H.; Jiang, P.; Dong, X.; Shi, J. *Chem. Mater*. **2007**, *19*, 4322.

(11) Knowles, J. C.; Bonfield, W. *J. Biomed. Mater. Res.* **1993**, *27*, 1591.

(12) Aryal, S.; Bhattarai, S. R.; Bahadhur, K. C. R.; Khil, M. S.; Lee, D. R.; Kim, H. Y. *Mater. Sci. Eng. A* **2006**, *426*, 202.

(13) Elliott, J. C.; Mackie, P. E.; Young, R. A. *Science* **1973**, *180*, 1055.

(14) Oyane, A.; Kim, H. M.; Furuya, T.; Kokubo, T.; Miyazaki, T.; Nakamura, T. *J. Biomed. Mater. Res.* **2003**, *65A*, 188.

(15) Sun, X.; Liu, J.; Li, Y. *Chem. Eur. J.* **2006**, *12*, 2039.

(16) Dinesh, J.; Eswaramoorthy, M.; Rao, C. N. R. *J. Phys. Chem. C* **2007**, *111*, 510.

(17) Shi, Q.; Wang, J.; Zhang, J.; Fan, J.; Stucky, G. D. *Adv. Mater*. **2006**, *18*, 1038.

(18) Yan, H.; Zhang, K.; Blanford, C. F.; Francis, L. F.; Stein, A. *Chem. Mater*. **2001**, *13*, 1374.